The Journal of Chemical Physics

RESEARCH ARTICLE | AUGUST 22 2023

Solvation of furfural at metal–water interfaces: Implications for aqueous phase hydrogenation reactions

Special Collection: 2023 JCP Emerging Investigators Special Collection

Sihang Liu ; Sudarshan Vijay ; Mianle Xu ; Ang Cao ; Hector Prats ; Georg Kastlunger ; Hendrik H. Heenen ; Nitish Govindarajan

J. Chem. Phys. 159, 084702 (2023)
https://doi.org/10.1063/5.0157573

AIP Publishing

The Journal of Chemical Physics ARTICLE pubs.aip.org/aip/jcp

Solvation of furfural at metal–water interfaces: Implications for aqueous phase hydrogenation reactions

Cite as: J. Chem. Phys. 159, 084702 (2023); doi: 10.1063/5.0157573
Submitted: 9 May 2023 • Accepted: 21 June 2023 •
Published Online: 22 August 2023

Sihang Liu,[1] Sudarshan Vijay,[1,a)] Mianle Xu,[1] Ang Cao,[1] Hector Prats,[1,2] Georg Kastlunger,[1] Hendrik H. Heenen,[1,3] and Nitish Govindarajan[1,4,b)]

AFFILIATIONS

[1] Catalysis Theory Center, Department of Physics, Technical University of Denmark (DTU), 2800 Kgs. Lyngby, Denmark
[2] Department of Chemical Engineering, University College London, Roberts Building, Torrington Place, London WC1E 7JE, United Kingdom
[3] Fritz-Haber-Institut der Max-Planck-Gesellschaft, Berlin 14195, Germany
[4] Materials Science Division, Lawrence Livermore National Laboratory, Livermore, California 94550, USA

Note: This paper is part of the 2023 JCP Emerging Investigators Special Collection.
[a)] **Present address:** Department of Materials Science and Engineering, University of California, Berkeley, Berkeley, California 94720, USA and Materials Science Division, Lawrence Berkeley National Laboratory, Berkeley, California 94720, USA.
[b)] **Author to whom correspondence should be addressed:** govindarajan1@llnl.gov

ABSTRACT

Metal–water interfaces are central to understanding aqueous-phase heterogeneous catalytic processes. However, the explicit modeling of the interface is still challenging as it necessitates extensive sampling of the interfaces' degrees of freedom. Herein, we use *ab initio* molecular dynamics (AIMD) simulations to study the adsorption of furfural, a platform biomass chemical on several catalytically relevant metal–water interfaces (Pt, Rh, Pd, Cu, and Au) at low coverages. We find that furfural adsorption is destabilized on all the metal–water interfaces compared to the metal–gas interfaces considered in this work. This destabilization is a result of the energetic penalty associated with the displacement of water molecules near the surface upon adsorption of furfural, further evidenced by a linear correlation between solvation energy and the change in surface water coverage. To predict solvation energies without the need for computationally expensive AIMD simulations, we demonstrate OH binding energy as a good descriptor to estimate the solvation energies of furfural. Using microkinetic modeling, we further explain the origin of the activity for furfural hydrogenation on intrinsically strong-binding metals under aqueous conditions, i.e., the endothermic solvation energies for furfural adsorption prevent surface poisoning. Our work sheds light on the development of active aqueous-phase catalytic systems via rationally tuning the solvation energies of reaction intermediates.

INTRODUCTION

Adsorption of molecules at solid–gas and solid–liquid interfaces is the heart of heterogeneous catalysis.[1] Adsorption energy scaling relationships have widely been used to understand the trends in catalytic activity and selectivity, providing valuable insights for mechanistic studies and catalyst design.[2–7] Although great progress has been made to understand the adsorption phenomena of various adsorbate species at solid–gas interfaces, the adsorption of species in the presence of solvents, e.g., water, is less studied. This knowledge gap exists although the solvent has been shown to play a significant role in governing the reactivity of heterogeneous catalysts at the solid–liquid interface.[8,9] The inadequate understanding of solvent effects on the adsorption of reaction intermediates hinders the transferability of acquired knowledge of a vast majority of catalytic reactions in the gas phase to their liquid-phase counterparts.

Furfural (FCHO, where F denotes the furan ring and CHO denotes the aldehyde group) is an important platform molecule derived from lignocellulose, with widespread application in polymer

and biofuel synthesis.[10,11] Annually, more than 60% of produced furfural is used to produce furfuryl alcohol (FCH_2OH), a key monomer to synthesize furan resins, via catalytic hydrogenation.[12] Both heterogeneous gas(vapor)- and liquid-phase furfural hydrogenation have widely been studied,[13,14] with the latter having the advantages of operating under relatively milder conditions and having a higher yield[15,16] with a tunable selectivity toward the desired products.[17] In particular, solvents, such as water, enable hydrogenation reactions on Pt-group metals even at room temperature. For instance, Pt could catalyze furfural hydrogenation selectively to furfuryl alcohol at 323 K in methanol[18] and 303 K in aqueous phase.[19] Ru has even been shown to achieve nearly 100% selectivity to furfuryl alcohol at 293 K in aqueous phase.[20] In contrast, the hydrogenation reaction at a solid–gas interface necessitates high temperatures on a Pt surface.[21] The origin of the increased activity and selectivity in aqueous phase has been attributed to different solvent effects,[22] including the solvent acting as a co-catalyst[23] or a promoter,[24] the opening of new reaction channels in the presence of the solvent,[25] and the solvent acting as a reactant,[26] e.g., as a proton donor.[27] The deviating strands in reasoning emphasize the need for the atomistic level understanding of the interaction of biomass-derived molecules, such as furfural, on metal–water interfaces.

In heterogeneous furfural hydrogenation at a solid–water interface, FCHO interacts not only with the catalyst surface but also with the surrounding water molecules, which can affect its adsorption properties and the catalytic activity. For instance, combining experimental isotherms and density functional theory (DFT) calculations, Akinola *et al.* revealed that the adsorption of large organic molecules (including FCHO) is weakened on strong-binding surfaces, such as Pt and Rh, in aqueous phase compared to ultra-high vacuum (UHV) conditions. This weakening is attributed to the large enthalpic penalty associated with water displacement at the metal–water interface upon the adsorption of large organic molecules.[28] The weakened adsorption under aqueous conditions can also help explain the origin of the activity (at room temperature) for the hydrogenation of these large organic molecules on such strong-binding surfaces. Based on the solution calorimetry results[29] and previous thermodynamic cycle approaches,[30] Singh and Campbell proposed a simple bond-additivity model to quantify the energetic penalty for the adsorption of (flat) aromatic molecules on metal surfaces, which has mainly been attributed to water displacement during the adsorption of these large aromatic molecules.[31] However, the as-proposed methods strongly rely on indirect electrochemical measurements and isotherm adsorption models, which might suffer from uncertainties in the estimated results.

Ab initio molecular dynamics (AIMD) provides direct atomistic level insights into the adsorption phenomena and catalysis at metal–water interfaces.[32–38] For instance, Heenen *et al.* studied the adsorption of several common adsorbates (CO^*, CHO^*, COH^*, $OCCHO^*$, OH^*, and OOH^*) on Cu, Au, and Pt metal–water interfaces and found the solvation energies to be dependent on both the identity of the adsorbate and the metal surface. As a result, the estimated solvation energies for the adsorbates are non-transferable across metal surfaces, e.g., CO^* adsorption energy is barely affected by the presence of water on most of the metal (111) surfaces but slightly weakened on (211) surfaces,[39] while OH adsorption shows over 0.5 eV stabilization in aqueous phase (compared to vacuum) on Au(111) and Pt(111).[40] In contrast, Yoon *et al.* reported the adsorption of phenol on metal–water interfaces to be consistently destabilized on Pt(111) and Ni(111).[41] Zare *et al.* developed a hybrid quantum mechanical/molecular mechanical (QM/MM) approach to find that the adsorption of large molecules, i.e., benzene and phenol, is dramatically weakened on Pt(111) and Cu(111) in aqueous phase at 298 K, as a result of large endergonic cavity formation energy.[42] A recent work by Yao *et al.* has demonstrated the adsorption of furfural at the Cu(111)–water interface, which displays a tendency to adsorb rather than desorb into water at 443 K.[43] However, most of the previous studies on biomass related processes focus on a limited number of (metal) catalysts (usually only one), making it hard to obtain generalizable conclusions. In summary, the adsorption of small molecules in aqueous phase could be either destabilized or stabilized compared to vacuum/gas conditions, while larger molecules tend to suffer from huge energetic penalties associated with the replacement of water molecules (cavity formation) in aqueous phase.

Herein, we systematically study the adsorption of furfural based on AIMD simulations at 300 K for five metal–water interfaces, i.e., Au(111), Cu(111), Pd(111), Pt(111), and Rh(111) (cf. Scheme 1), which have extensively been investigated for furfural valorization.[13,26] The computed furfural adsorption on these surfaces is consistently destabilized under aqueous conditions compared to vacuum conditions, i.e., the solvation energies (ΔE_{sol}) of furfural are positive in all cases. Our AIMD results show good agreement with previous solution calorimetry[28,44] and thermodynamic cycle models.[31] The structural analyses of the metal–water interfaces from AIMD simulations suggest that the positive solvation energies are due to the energetic penalty associated with the displacement of surface adsorbed water molecules due to furfural adsorption, evidenced by a strong correlation between the solvation energy and surface water replacement. Importantly, we find the hydroxyl (OH) binding energy to be a descriptor for the solvation energy of furfural at metal–water interfaces, which bypasses the need for expensive AIMD simulations to obtain solvation energies. In addition, we discuss the differences in the origin of the endothermic solvation energies for furfural at metal–water interfaces between

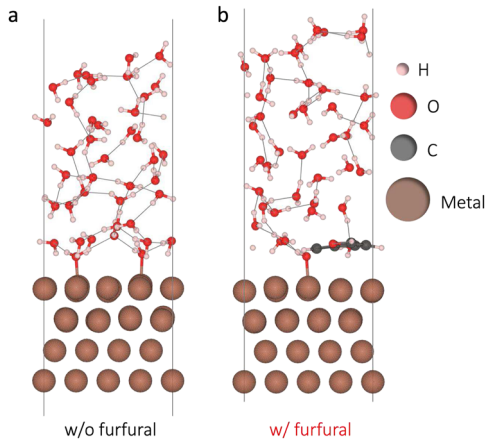

SCHEME 1. A schematic of the various metal [Au, Cu, Pt, Pd, and Rh(111)]–water interface models studied using AIMD simulations. (a) Without furfural adsorption and (b) with furfural adsorption. The color coding for the atoms is shown on the right.

the bond-additivity model and the AIMD simulations. Based on a simple microkinetic model developed in our previous study,[14] we show that the endothermic solvation energies promote the furfural hydrogenation reaction toward furfuryl alcohol on strong-binding metals. This study generalizes the solvent effects on furfural adsorption across different metal surfaces via simple scaling relations and provides a rationale for screening both catalysts and solvents to promote the catalytic activity of furfural hydrogenation and other biomass valorization reactions.

COMPUTATIONAL METHODS

DFT calculations

The Vienna *Ab initio* Simulation Package (VASP)[45] was used in this work to perform DFT and AIMD simulations using the revised Perdew–Burke–Ernzerhof (RPBE)[46] exchange–correlation (XC) functional complemented with the D3 dispersion correction[47,48] that has previously been used in the simulations of metal–water interfaces.[49] A plane-wave cutoff of 400 eV and a Gaussian smearing of width 0.2 eV were used in all the simulations. The electronic structure was relaxed until all forces converged to less than 0.05 eV/Å for geometry optimizations.

The metal surfaces were modeled as 4 × 4 × 4 Au, Cu, Pd, Pt, and Rh fcc(111) slabs, which are commonly used as catalysts in thermal furfural hydrogenation.[13] The top two layers of the metal surfaces were relaxed, while the bottom two were fixed to their bulk structures, with optimized lattice constants of 4.17, 3.58, 3.92, 3.94, and 3.80 Å, respectively. A 3 × 3 × 1 k-point mesh was applied on all surfaces. As for furfural adsorption, one furfural molecule in the unit cell with 16 surface metal atoms was used in the simulations. Both upright and flat adsorption configurations of furfural were considered in vacuum calculations, with the flat configuration being much more stable than the upright configuration, in line with a previous report.[14] We investigated the dependence of furfural adsorption energies on surface size at the metal–vacuum interface as shown in Fig. S1 and found out that the 4 × 4 slab model is representative of furfural adsorption in the low coverage regime. Since we find furfural in this study to be only weakly solvated and to, thus, have a negligible solvation shell, we expect this size dependency to hold in an aqueous environment. The static binding energy of furfural in vacuum is obtained using Eq. (1),

$$\Delta E_{FCHO} = E_{slab\_FCHO} - E_{slab} - E_{FCHO(g)}. \quad (1)$$

An OH molecule on the top site of all metal surfaces is simulated to obtain the static vacuum OH binding energies using Eq. (2),

$$\Delta E_{OH} = E_{slab\_OH} - E_{slab} - \left(E_{H_2O(g)} - 0.5E_{H_2(g)}\right), \quad (2)$$

where the gas-phase energies of the reference gases, such as FCHO(g), H_2O(g), and H_2(g), are calculated using static DFT calculations.

AIMD simulations

AIMD simulations were performed with a 0.5 fs time step employing a Nosé thermostat set at 300 K. Forty water molecules were included in the metal–water interfaces for the fcc(111) surfaces, corresponding to roughly five layers of the aqueous solvent. A furfural molecule was placed on the metal surface surrounded by water to simulate FCHO adsorption at the metal–water interfaces. The AIMD-based vacuum adsorption energy $\Delta E_{FCHO\_vac\_AIMD}$, the aqueous-phase adsorption energy $\Delta E_{FCHO\_aq\_AIMD}$, and the solvation energy ΔE_{solv} against the adsorption in vacuum were calculated as follows:

$$\Delta E_{FCHO\_vac\_AIMD} = E_{slab\_FCHO\_vac\_AIMD} - E_{slab\_vac\_AIMD} - E_{FCHO(g)\_AIMD}, \quad (3)$$

$$\Delta E_{FCHO\_aq\_AIMD} = E_{slab\_FCHO\_aq\_AIMD} - E_{slab\_aq\_AIMD} - E_{FCHO(g)\_AIMD}, \quad (4)$$

$$\Delta E_{solv} = \Delta E_{FCHO\_aq\_AIMD} - \Delta E_{FCHO\_vac\_AIMD}, \quad (5)$$

where $E_{FCHO(g)\_AIMD}$ is the gas energy of a furfural molecule derived from AIMD simulations at 300 K with a 3/2 k_BT correction, because the center of mass (COM) motions are not included in the gas-phase AIMD simulations.[50,51] Three independent trajectories were simulated out for each aqueous system with randomly generated starting configurations of the solvent water molecules. To determine the uncertainty in the measured quantities, we report the standard deviation σ as error bars obtained from the trials as $\frac{\sigma}{\sqrt{n}}$, where $n = 3$. Each AIMD trajectory was run for 50–70 ps after a pre-equilibration period of ~5 ps. We ensured that the individual trajectories are converged, showing an average drift in the total energy of <0.05 eV/ps after equilibration, as shown in Fig. S2. The last 10 ps of three parallel converged trajectories of each system was used as statistics to probe the converged energetics and structural properties. The z-axis distribution of water molecules was estimated using either the O or the H atoms of H_2O. As shown in Fig. S3, on the studied metal surfaces, our simulation configurations reproduce the physical interfaces where the water in the region of 5–10 Å reaches the density of liquid water,[52,53] denoted by the blue dashed lines. The residence time of furfural chemisorption is analyzed via a "surface metal atom–furfural atom" pair count based on a cutoff criterion shown in Table S1 and explained, in more detail, in the supplementary material.

The water molecule is considered to be adsorbed on the surface if it is closer than 2.55 Å to a surface metal atom as suggested by Heenen *et al.* based on analyzing the radial distribution functions of the metal–water interface.[40] To account for the different covalent radii of metal atoms, we re-estimated the chemisorbed water based on $r_{H2O,Metal}$ (the atomic distance between surface metal atoms and O in H_2O) in reference to Cu(111) $r_{H2O,Cu}$ = 2.55 Å calculated from metal–water radial distribution functions (RDFs),[40]

$$r_{H_2O,Metal} = 2.55\text{Å} \times \frac{r_{cov,metal} + r_{cov,O}}{r_{cov,Cu} + r_{cov,O}}, \quad (6)$$

with the covalent radii r_{cov} = 0.66, 1.32, 1.36, 1.39, 1.36, and 1.42 Å for O, Cu, Au, Pd, Pt, and Rh, respectively, derived from Ref. 54.

The surface water coverage θ_w was calculated by averaging the total number of adsorbed H_2O molecules $\langle\widetilde{n_w}\rangle$ during an AIMD trajectory and normalizing this value by the number of surface atoms per unit cell (16) as shown in Eq. (7),

$$\theta_w = \frac{\langle\widetilde{n_w}\rangle}{16}. \quad (7)$$

The hydrogen bonds formed between the adsorbed furfural and water were explicitly counted by the distance and angle criteria for the bonding of O/H in furfural and H/O in H_2O as reported in Ref. 55. The major post-processing results are summarized in Table S2 of the supplementary material. The analysis functions and methodologies to obtain all energetic and structural results from the AIMD simulations are available in the AIMDprobe package: https://github.com/tjunewson/AIMDprobe.

RESULTS AND DISCUSSION

Adsorption of furfural results in the decreased surface coverage of water at the metal–water interface

Furfural demonstrates different adsorption behaviors at the studied metal–water interfaces. In general, furfural binds flatly to all metal surfaces occupying ~5 metal atoms as displayed in Fig. S4 and does not desorb into the water bulk within the timescales of the AIMD simulations [cf. time resolution of center of mass (COM) in Fig. S5]. A detailed analysis points to the distinct differences in the adsorption configurations of furfural, which indicate an increasing binding strength following the trend Au < Cu < Pd ≈ Pt ≈ Rh. In a first instance, this is evident by the adsorption height (in the z direction) to the respective metal surfaces described by the distance between the COM of furfural and the metal surface as shown in Table S2.

The COM–surface distance, denoted by the vertical dotted lines in Fig. 1, shows that the furfural is located within the first water layer for the strong-binding metals, such as Pd, Pt, and Rh, and resides slightly above the first water layer [the peaks shown in Figs. 1(a) and 1(b) for Au and Cu, respectively]. These adsorption heights are accompanied by a complete immobility for Pd, Pt, and Rh and moderate and high lateral mobilities for Cu and Au, respectively [cf. furfural's mean square displacement (MSD) in Fig. S6]. Using the metal atom residence time distribution shown in Fig. S7, we can finally conclude that the furfural directly chemisorbs on Pd, Pt, and Rh, through the C atoms in the furan ring, while the –CHO group is pointing to the water on Pd and Pt and binding to Rh via its O. In comparison, a weak physisorption is found for Cu, which is evident through a sole interaction of the –CHO group's O atom resulting in a tilted adsorption geometry. No specific interaction of furfural with Au is found, indicating that its adsorption above the first water layer is entropy driven, which is a typical behavior for hydrophobic adsorbates.[56,57]

Interestingly, we find these adsorption geometries of low-coverage furfural at the metal–water interfaces to resemble those at metal–gas interfaces (Fig. S4, upper and lower panels) and those in previous studies,[58–62] i.e., a flatly adsorbed orientation on Pt-group metals, a flat (weakly interacting) orientation on Au, and a slightly tilted orientation on Cu. We further show in Table S3 that the calculated centers of mass (COM) of furfural at the metal–water interfaces are very close to those at metal–vacuum interfaces. These results

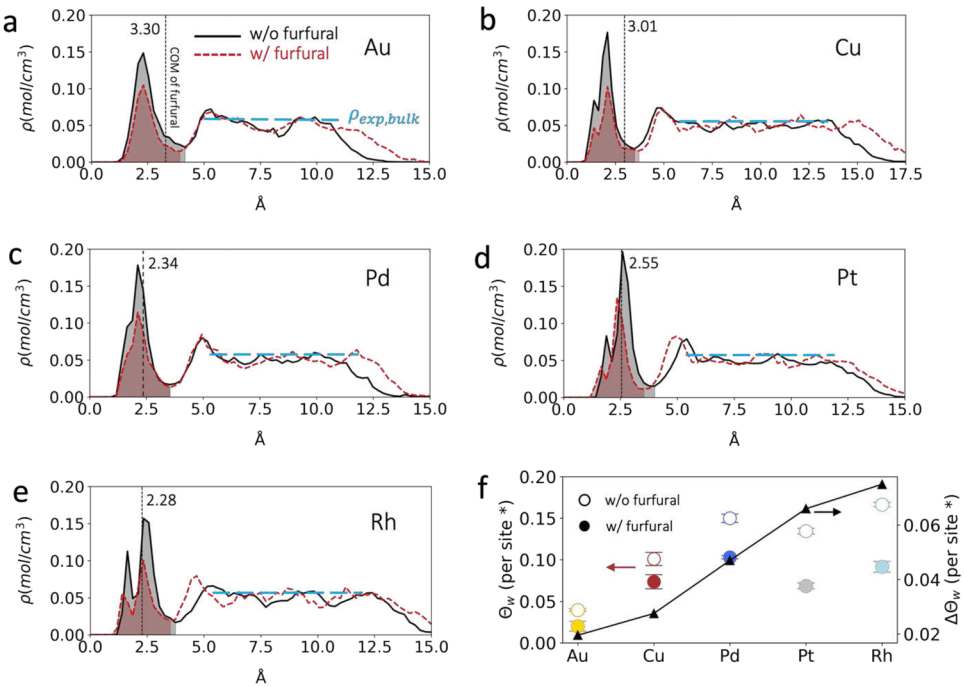

FIG. 1. Water density profiles obtained from the AIMD simulations of the different metal–water interfaces. (a) Au(111), (b) Cu(111), (c) Pd(111), (d) Pt(111), and (e) Rh(111); (f) the site-normalized surface water coverage without furfural adsorption (left axis) and the change with furfural adsorption (right axis). Note that water molecules are located based on the position of the oxygen atom. The vertical dotted lines in (a)–(e) highlight the centers of mass of furfural. The blue dashed lines denote the experimental density of bulk water at room temperature.

suggest that solvent water might not affect the adsorption geometries of hydrophobic adsorbates on metal surfaces.

The averaged distribution of water molecules before and after furfural adsorption shows notable water replacement, especially near the surface (<5 Å) [cf. Figs. 1(a)–1(e)]. The density of water is the highest near the metal–water interface due to the adsorption of water molecules on the surface and consequent local crowding. The liquid–vapor interfaces on Cu are the highest (~15 Å) among the studied surfaces as shown in Fig. 1(b) due to its smallest lattice constant among the studied metals. Note that except for the Au surface, shown in Fig. 1(a), all metal surfaces display a small shoulder peak to the left of the major peak, which originates from the fact that the first layer of water molecules binds to the surfaces mainly via the O atoms. This adsorption results in H atoms pointing outward the surface to form an O-void in the second water layer, i.e., the typical bilayer structure of water on reactive metal surfaces.[63]

As shown in Fig. 1(f), we find that from Au to Rh, the site-normalized surface water coverages (θ_w) generally increase, in line with a previous report.[40] We note that the calculated water coverage on Pt(111) shows good quantitative agreement with previous AIMD studies (with different surface sizes) performed using the RPBE-D3 functional (cf. Table S4). Calculations by Le *et al.* predict slightly higher water coverages,[64,65] which is likely due to the stronger binding of water by the PBE-D3 functional.[66] More importantly, the replaced water coverages upon furfural adsorption $\Delta\theta_w$ also increase from Au to Rh. Assuming that a furfural molecule occupies the same number of surface sites (~5)[31] on different metal surfaces at low coverages, we expect that the replaced water coverages should be dependent on the binding strength of water or correlated binding properties, such as the OH binding energy,[2] on the respective metal surfaces. We will return to this point later in this paper.

We further studied the formation of directional hydrogen bonds between the adsorbate (furfural) and solvent water, which could stabilize the adsorption.[67] The cumulative averages of calculated hydrogen bonds formation between furfural and water are summarized in Table S1 (the bond formation criteria are detailed in the section titled COMPUTATIONAL METHODS). We find that <1 hydrogen bond is formed per adsorbed furfural molecule with the solvent water molecules. This low degree of hydrogen bonding is comparable to the very weakly interacting CO* at the metal–water interfaces[40] and rules out the possible stabilization effects on furfural adsorption via hydrogen bond interactions at the metal–water interface.

Furfural adsorption is destabilized under aqueous conditions on metal surfaces

As shown in Fig. 2(a), the aqueous-phase adsorption energies of furfural at the metal–water interfaces estimated from the AIMD simulations are all weaker than the corresponding adsorption energies in vacuum, i.e., the solvation energies of furfural on the metal surfaces are endothermic as can be seen in Fig. 2(b). Notably, the estimated adsorption energies from the AIMD simulations for Pt and Rh are in good agreement with the solution calorimetry experiments[28,29] and the bond-additivity model.[31] The calculated solvation energies for the studied metal–water interfaces are all above +0.4 eV and reach up to +1 eV on Pt and Rh, far beyond the DFT intrinsic error of ~0.2 eV on calculated adsorption

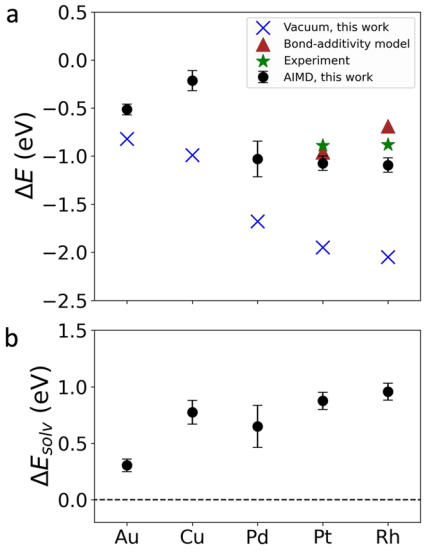

FIG. 2. Determined adsorption energies for furfural (a) in vacuum, AIMD simulations, experiments,[28] and the bond-additivity model;[28] (b) the solvation energy for furfural on the studied surfaces estimated using the AIMD simulations. The standard deviations are obtained from three independent simulation trajectories for each of the studied metal–water interfaces.

energies,[68] which should have a considerable impact on the adsorption phenomena and catalytic processes related to furfural under aqueous conditions. Furthermore, we find that the bond-additivity model[31] and AIMD simulations in this work estimate similar solvation energies of furfural on the Pt(111) surface of ~0.72 and 0.82 eV, respectively [cf. Fig. 2(a)]. However, we note that there are important differences in their origin as discussed in Fig. S8 in the supplementary material.

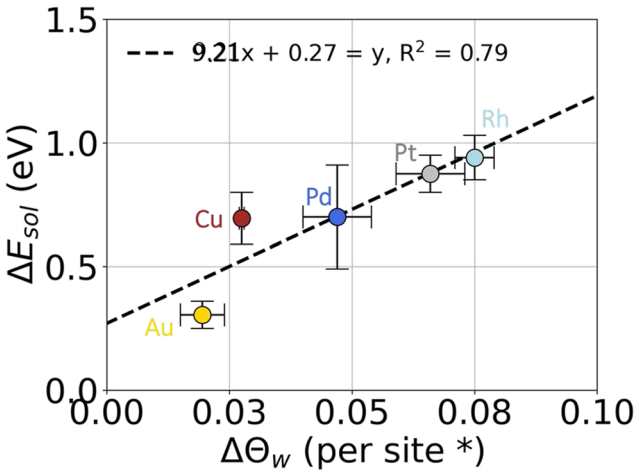

FIG. 3. Correlation between the AIMD-derived furfural solvation energies at the metal–water interfaces and the replaced surface water coverages (per surface site).

To shed light on the origin of the endothermic solvation energies, we further plot the solvation energies of furfural adsorption against the replaced surface water coverages as shown in Fig. 3. We find that the solvation penalty linearly increases with increasing number of replaced water molecules per site. This universal correlation strongly suggests that the destabilization of furfural adsorption at metal–water interfaces should be a result of the energetic penalty associated with the displacement of water molecules near the surface due to the introduction of a large molecule, such as furfural. We note in passing that the intercept of the linear relationship in Fig. 3 is positive (+0.27 eV), indicating an intrinsic destabilization of furfural adsorption at the metal–water interface even in the absence of competitive water adsorption.

OH binding energy is a good descriptor to predict solvation energies and circumvent expensive AIMD simulations

The identification of simple descriptors to predict critical quantities for metal–water interfaces can be very useful for the rational design of new catalysts without the need for computationally expensive simulations.[4] For instance, Kelly *et al.* proposed OH binding energies to universally correlate with both potentials of zero charge and site-normalized water coverages on a number of transition metal surfaces.[69] In addition, the OH binding energies have been applied to predict the solvation energy of OH adsorption in aqueous phase.[40] Similarly, H_2O binding energies have been shown to predict the Volta potential difference between the surface of metal and water.[70]

Inspired by the aforementioned studies on identifying simple descriptors, we find that the OH binding energies scale well with the solvation energies of furfural on the studied metal surfaces (cf. Fig. 4). A stronger binding of OH gives rise to more endothermic solvation energies, i.e., weaker binding of furfural. The linear correlation between the OH binding energy and furfural solvation energy in aqueous phase can be used to obtain a reasonable estimate of the solvation energies on different metal surfaces, hence allowing the estimation of aqueous-phase adsorption energies of furfural on metal surfaces without the need for expensive AIMD simulations. We expect that this simple descriptor can be used to estimate the energetic penalty associated with water replacement for other hydrophobic species, e.g., furan and benzene, but with different scaling relations due to differences in the nature of the metal–adsorbate interaction. In contrast to hydrophobic molecules, glycerol and other biomass derivatives with one or more –OH groups can form complicated hydrogen bond networks with protic solvents, such as water. This necessitates a more robust sampling of possible adsorption configurations for such molecules at metal–solvent interfaces. Therefore, more complicated relationships might be required to account for stabilizing effects, e.g., a separate term/descriptor to account for the energetics of hydrogen bond formation to predict the solvation energies of biomass related species containing –OH groups [e.g., glycerol and 5-hydroxymethylfurfural (HMF)] in polar, protic solvents.

Before closing this section, we would like to highlight a few shortcomings of this work. First, the AIMD simulations were only performed for the (111) surfaces of the metals considered in this study. Thereby, the trends in solvation energies on other high-index surfaces might be different to the ones observed in this work. Second, the timescales accessible by AIMD simulations are limited because of the expensive energy and force estimates needed for each timestep. The nanosecond timescales that might be needed for sufficient sampling of metal–water interfaces[71] are currently out of reach for AIMD simulations. This could be resolved in future studies by employing machine learning based interatomic potentials to perform long timescale molecular dynamics simulations of metal–water interfaces.[71–74] However, the reasonable agreement of our determined solvation energies on Pd and Pt with experimentally determined values gives us confidence in the validity of the results.

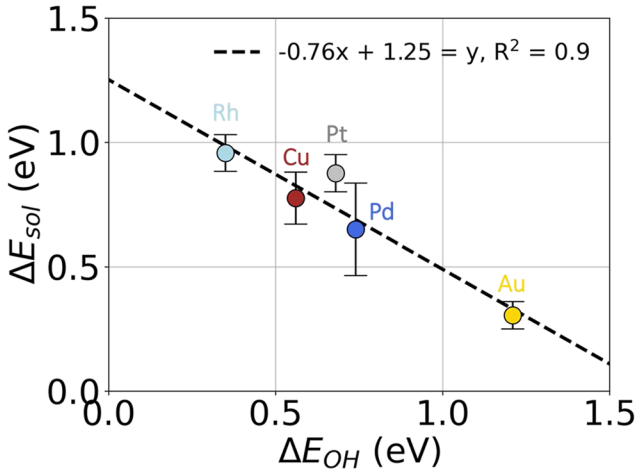

FIG. 4. Scaling relationship between the AIMD-derived furfural solvation energies at the metal–water interfaces and the calculated OH binding energies in vacuum.

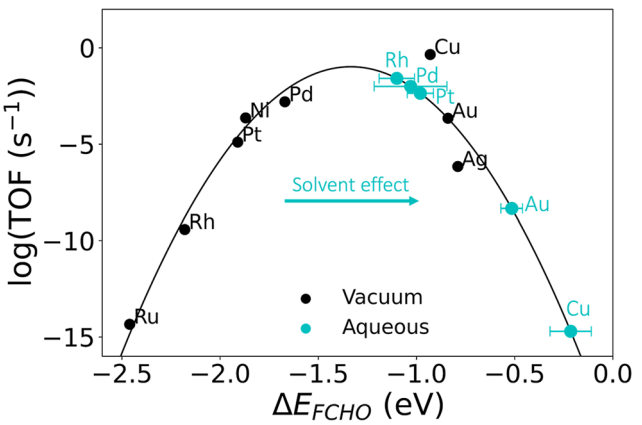

FIG. 5. Theoretical activity volcano for furfural hydrogenation to furfuryl alcohol at 300 K on different (111) metal surfaces under gas (black markers) and aqueous conditions based on solvation energies obtained from the AIMD simulations of the metal–water interfaces considered in this work (cyan markers).

Endothermic solvation energies activate furfural hydrogenation on strong-binding metals by preventing surface poisoning

To demonstrate the implications of the differences in the adsorption energies of furfural under gas- and aqueous-phase conditions, we studied the hydrogenation of furfural toward furfuryl alcohol, a central reaction for furfural valorization.[13,75] Pt(111) was used as an example to highlight the effect of the solvation energy corrections to the reaction energetics containing furanic species. As shown in Fig. S9, the reaction energy for furfural adsorption on Pt(111) is significantly weakened in the aqueous phase. We then performed microkinetic simulations for furfural hydrogenation to construct the activity volcano for several (111) transition metal surfaces (cf. Fig. 5). We note that the solvation energy estimated for furfural was used for all reaction intermediates in the microkinetic simulations based on the assumption of the similar size and hydrophilicity of furanic species along the reaction pathway to furfuryl alcohol (only the aldehyde group is hydrogenated). The activity volcano under gas-phase conditions (black markers in Fig. 5) indicates that strong-binding metals, e.g., Ru, Rh, and Pt, display very low activity at room temperature for furfural hydrogenation due to the surface poisoning of furanic intermediates, e.g., FCHO*, as shown by the simulated coverages (cf. Fig. S10). We find that the predicted catalytic activity for these strong-binding metals significantly increases if we consider the hydrogenation under aqueous conditions, where the furfural binding is greatly weakened due to the endothermic solvation energy (cyan markers in Fig. 5). In contrast, the weaker-binding metals, e.g., Au and Cu, suffer from the destabilization effect from solvation, which results in lower activities toward furfural hydrogenation. An important observation is the change in the most active metals predicted by the activity volcano under vacuum (coinage metals) and aqueous conditions (Pt-group metals).

The weakened adsorption of furanic species for the metals in the strong-binding leg of the volcano prevents surface poisoning and allows for sufficient coverage of H species, as shown in Fig. S10, which results in the increased activity for aqueous-phase hydrogenation. These results provide insights into the importance of aqueous conditions in catalyzing furfural hydrogenation on strong-binding metals at room temperatures and why Pt-group metals display activity in the electroreduction of furfural and other furanic reactants under aqueous conditions.[76] However, solvent-mediated mechanisms, such as H-shuttling,[25,43] possible hydrogen bond stabilization for other reaction intermediates, and high-index facets, have not been considered in the model. We postulate that the neglected stabilizing effects from both hydrogen bond formation and water-aided hydrogenation pathways on other reaction intermediates than furfural are likely to have lower energetic contributions relative to the solvation penalties resulting from water replacement, and their impact is, thus, minor. This assumption is particularly valid on stronger binding metals (Pd, Pt, and Rh). For the moderate and weak binding metals (Cu and Au), these stabilizing effects might play a bigger role in the overall aqueous-phase hydrogenation activity and compensate for the overall energetic penalty of solvation, which may, therefore, be overestimated in our study.

CONCLUSION

Understanding the adsorption phenomena at the metal–water interfaces aids in the optimization of reaction conditions for important aqueous-phase catalytic transformations. In this work, we studied the adsorption of furfural in aqueous phase, a platform biomass derivative, on several transition metal–water interfaces using AIMD simulations. Our work estimates large endothermic solvation energies associated with furfural adsorption on metal–water interfaces, which we attribute to the replacement of surface adsorbed water molecules in the presence of furfural. The linear correlation between the solvation energies and replaced water coverages further confirms the origin of the endothermic solvation energies. To circumvent the need for expensive AIMD simulations of metal–water interfaces, we propose the OH adsorption energy of the transition metal to be a good descriptor to estimate the solvation energies of furfural. We further bridge the understanding of furfural hydrogenation between gas and aqueous conditions via a simple microkinetic model, which can help explain the origin of the activity of aqueous-phase furfural hydrogenation on Pt-group metals under mild conditions.

SUPPLEMENTARY MATERIAL

See the supplementary material for the convergence and major results of AIMD simulations, details of the microkinetic model, the coverage-dependent furfural adsorption energy, the snapshots of furfural adsorption configurations, the time-averaged center of mass (COM) and mean squared displacement (MSD) of furfural, the cumulative residence time of furfural, the comparison between a previous bond-additivity model and AIMD simulations, and the simulated and fitted coverages in microkinetic modeling.

ACKNOWLEDGMENTS

S.L., M.X., H.P., and N.G. were supported by a research grant (Grant No. 29450) from Villum Fonden. S.V., H.H.H., and G.K. were supported by a research grant (Grant No. 9455), V-Sustain, from Villum Fonden. S.L., S.V., G.K., and N.G. acknowledge PRACE for awarding them access to the JUWELS supercomputer in Jülich, Germany, and VEGA supercomputers in IZUM Maribor, Slovenia through Project No. 2020235596. N.G. wrote the manuscript under the auspices of the U.S. Department of Energy by Lawrence Livermore National Laboratory (LLNL) under Contract No. DE-AC52-07NA27344. We thank Karen Chan for the insightful discussions in the early stages of this work.

AUTHOR DECLARATIONS

Conflict of Interest

The authors have no conflicts to disclose.

Author Contributions

Sihang Liu: Conceptualization (equal); Data curation (equal); Formal analysis (lead); Investigation (lead); Methodology (equal); Validation (equal); Visualization (equal); Writing – original draft (lead);

Writing – review & editing (lead). **Sudarshan Vijay**: Investigation (supporting); Writing – review & editing (supporting). **Mianle Xu**: Investigation (supporting); Writing – review & editing (supporting). **Ang Cao**: Writing – review & editing (supporting). **Hector Prats**: Formal analysis (supporting); Investigation (supporting); Writing – review & editing (supporting). **Georg Kastlunger**: Investigation (supporting); Supervision (supporting); Writing – review & editing (supporting). **Hendrik H. Heenen**: Supervision (supporting); Writing – review & editing (supporting). **Nitish Govindarajan**: Conceptualization (equal); Formal analysis (equal); Investigation (equal); Project administration (lead); Resources (equal); Supervision (lead); Visualization (equal); Writing – original draft (equal); Writing – review & editing (equal).

DATA AVAILABILITY

The raw data and scripts needed to reproduce the figures in the manuscript are openly available in the CatTheory GitHub repository at https://github.com/CatTheoryDTU/furfural_solvation_AIMD.

REFERENCES

[1] J. K. Nørskov, F. Studt, F. Abild-Pedersen, and T. Bligaard, *Fundamental Concepts in Heterogeneous Catalysis* (Wiley, Hoboken, NJ, 2015).

[2] F. Abild-Pedersen, J. Greeley, F. Studt, J. Rossmeisl, T. R. Munter, P. G. Moses, E. Skúlason, T. Bligaard, and J. K. Nørskov, "Scaling properties of adsorption energies for hydrogen-containing molecules on transition-metal surfaces," Phys. Rev. Lett. **99**(1), 016105 (2007).

[3] E. M. Fernández, P. G. Moses, A. Toftelund, H. A. Hansen, J. I. Martínez, F. Abild-Pedersen, J. Kleis, B. Hinnemann, J. Rossmeisl, T. Bligaard, and J. K. Nørskov, "Scaling relationships for adsorption energies on transition metal oxide, sulfide, and nitride surfaces," Angew. Chem., Int. Ed. **47**(25), 4683–4686 (2008).

[4] Z.-J. Zhao, S. Liu, S. Zha, D. Cheng, F. Studt, G. Henkelman, and J. Gong, "Theory-guided design of catalytic materials using scaling relationships and reactivity descriptors," Nat. Rev. Mater. **4**(12), 792–804 (2019).

[5] S. Vijay, G. Kastlunger, K. Chan, and J. K. Nørskov, "Limits to scaling relations between adsorption energies?," J. Chem. Phys. **156**(23), 231102 (2022).

[6] S. Liu, C. Yang, S. Zha, D. Sharapa, F. Studt, Z.-J. Zhao, and J. Gong, "Moderate surface segregation promotes selective ethanol production in CO_2 hydrogenation reaction over CoCu catalysts," Angew. Chem. **134**(2), e202109027 (2022).

[7] S. Liu, Z.-J. Zhao, C. Yang, S. Zha, K. M. Neyman, F. Studt, and J. Gong, "Adsorption preference determines segregation direction: A shortcut to more realistic surface models of alloy catalysts," ACS Catal. **9**(6), 5011–5018 (2019).

[8] L. Lin, Y. Ge, H. Zhang, M. Wang, D. Xiao, and D. Ma, "Heterogeneous catalysis in water," JACS Au **1**(11), 1834–1848 (2021).

[9] G. Gonella, E. H. G. Backus, Y. Nagata, D. J. Bonthuis, P. Loche, A. Schlaich, R. R. Netz, A. Kühnle, I. T. McCrum, M. T. M. Koper, M. Wolf, B. Winter, G. Meijer, R. K. Campen, and M. Bonn, "Water at charged interfaces," Nat. Rev. Chem. **5**(7), 466–485 (2021).

[10] R. Mariscal, P. Maireles-Torres, M. Ojeda, I. Sádaba, and M. López Granados, "Furfural: A renewable and versatile platform molecule for the synthesis of chemicals and fuels," Energy Environ. Sci. **9**(4), 1144–1189 (2016).

[11] S. Chen, R. Wojcieszak, F. Dumeignil, E. Marceau, and S. Royer, "How catalysts and experimental conditions determine the selective hydroconversion of furfural and 5-hydroxymethylfurfural," Chem. Rev. **118**(22), 11023–11117 (2018).

[12] A. Mandalika, L. Qin, T. K. Sato, and T. Runge, "Integrated biorefinery model based on production of furans using open-ended high yield processes," Green Chem. **16**(5), 2480–2489 (2014).

[13] Y. Wang, D. Zhao, D. Rodríguez-Padrón, and C. Len, "Recent advances in catalytic hydrogenation of furfural," Catalysts **9**(10), 796 (2019).

[14] S. Liu, N. Govindarajan, and K. Chan, "Understanding activity trends in furfural hydrogenation on transition metal surfaces," ACS Catal. **12**, 12902–12910 (2022).

[15] J. N. Chheda, G. W. Huber, and J. A. Dumesic, "Liquid-phase catalytic processing of biomass-derived oxygenated hydrocarbons to fuels and chemicals," Angew. Chem., Int. Ed. **46**(38), 7164–7183 (2007).

[16] J. C. Serrano-Ruiz, R. Luque, and A. Sepúlveda-Escribano, "Transformations of biomass-derived platform molecules: From high added-value chemicals to fuels via aqueous-phase processing," Chem. Soc. Rev. **40**(11), 5266 (2011).

[17] Y. Deng, R. Gao, L. Lin, T. Liu, X.-D. Wen, S. Wang, and D. Ma, "Solvent tunes the selectivity of hydrogenation reaction over α-MoC catalyst," J. Am. Chem. Soc. **140**(43), 14481–14489 (2018).

[18] M. Chatterjee, A. Chatterjee, T. Ishizaka, and H. Kawanami, "Defining Pt-compressed CO_2 synergy for selectivity control of furfural hydrogenation," RSC Adv. **8**(36), 20190–20201 (2018).

[19] G. Gao, J. Remón, Z. Jiang, L. Yao, and C. Hu, "Selective hydrogenation of furfural to furfuryl alcohol in water under mild conditions over a hydrotalcite-derived Pt-based catalyst," Appl. Catal., B **309**, 121260 (2022).

[20] J. Yang, J. Ma, Q. Yuan, P. Zhang, and Y. Guan, "Selective hydrogenation of furfural on Ru/Al-MIL-53: A comparative study on the effect of aromatic and aliphatic organic linkers," RSC Adv. **6**(95), 92299–92304 (2016).

[21] M. J. Taylor, L. Jiang, J. Reichert, A. C. Papageorgiou, S. K. Beaumont, K. Wilson, A. F. Lee, J. V. Barth, and G. Kyriakou, "Catalytic hydrogenation and hydrodeoxygenation of furfural over Pt(111): A model system for the rational design and operation of practical biomass conversion catalysts," J. Phys. Chem. C **121**(15), 8490–8497 (2017).

[22] G. Li, B. Wang, and D. E. Resasco, "Water-mediated heterogeneously catalyzed reactions," ACS Catal. **10**(2), 1294–1309 (2020).

[23] J. Saavedra, H. A. Doan, C. J. Pursell, L. C. Grabow, and B. D. Chandler, "The critical role of water at the gold-titania interface in catalytic CO oxidation," Science **345**(6204), 1599–1602 (2014).

[24] R. Ma, X.-P. Wu, T. Tong, Z.-J. Shao, Y. Wang, X. Liu, Q. Xia, and X.-Q. Gong, "The critical role of water in the ring opening of furfural alcohol to 1,2-pentanediol," ACS Catal. **7**(1), 333–337 (2017).

[25] Z. Zhao, R. Bababrik, W. Xue, Y. Li, N. M. Briggs, D.-T. Nguyen, U. Nguyen, S. P. Crossley, S. Wang, B. Wang, and D. E. Resasco, "Solvent-mediated charge separation drives alternative hydrogenation path of furanics in liquid water," Nat. Catal. **2**(5), 431–436 (2019).

[26] P. Nilges and U. Schröder, "Electrochemistry for biofuel generation: Production of furans by electrocatalytic hydrogenation of furfurals," Energy Environ. Sci. **6**(10), 2925 (2013).

[27] S. Liu, Z. Mukadam, S. B. Scott, S. Sarma, M.-M. Titirici, K. Chan, N. Govindarajan, I. E. L. Stephens, and G. Kastlunger, "Unraveling the reaction mechanisms for furfural electroreduction on copper," EES Catal. **1**, 539 (2023).

[28] J. Akinola, I. Barth, B. R. Goldsmith, and N. Singh, "Adsorption energies of oxygenated aromatics and organics on rhodium and platinum in aqueous phase," ACS Catal. **10**(9), 4929–4941 (2020).

[29] J. Akinola and N. Singh, "Temperature dependence of aqueous-phase phenol adsorption on Pt and Rh," J. Appl. Electrochem. **51**(1), 37–50 (2021).

[30] J. O'M. Bockris and K. Jeng, "In-situ studies of adsorption of organic compounds on platinum electrodes," J. Electroanal. Chem. **330**(1–2), 541–581 (1992).

[31] N. Singh and C. T. Campbell, "A simple bond-additivity model explains large decreases in heats of adsorption in solvents versus gas phase: A case study with phenol on Pt(111) in water," ACS Catal. **9**(9), 8116–8127 (2019).

[32] A. Groß and S. Sakong, "Ab initio simulations of water/metal interfaces," Chem. Rev. **122**, 10746 (2022).

[33] A. Hagopian, A. Falcone, M. Ben Yahia, and J.-S. Filhol, "*Ab initio* modelling of interfacial electrochemical properties: Beyond implicit solvation limitations," J. Phys.: Condens. Matter **33**(30), 304001 (2021).

[34] J.-B. Le, A. Chen, L. Li, J.-F. Xiong, J. Lan, Y.-P. Liu, M. Iannuzzi, and J. Cheng, "Modeling electrified Pt(111)-H_{ad}/water interfaces from ab initio molecular dynamics," JACS Au **1**(5), 569–577 (2021).

[35] X. Qin, T. Vegge, and H. A. Hansen, "Cation-coordinated inner-sphere CO_2 electroreduction at Au–water interfaces," J. Am. Chem. Soc. **145**(3), 1897–1905 (2023).

[36] M. C. O. Monteiro, F. Dattila, B. Hagedoorn, R. García-Muelas, N. López, and M. T. M. Koper, "Absence of CO_2 electroreduction on copper, gold and silver electrodes without metal cations in solution," Nat. Catal. **4**, 654–662 (2021).

[37]T. Ludwig, J. A. Gauthier, K. S. Brown, S. Ringe, J. K. Nørskov, and K. Chan, "Solvent–adsorbate interactions and adsorbate-specific solvent structure in carbon dioxide reduction on a stepped Cu surface," J. Phys. Chem. C **123**(10), 5999–6009 (2019).
[38]H. H. Kristoffersen, K. Chan, T. Vegge, and H. A. Hansen, "Energy–entropy competition in cation–hydroxyl interactions at the liquid water–Pt(111) interface," Chem. Commun. **56**(3), 427–430 (2020).
[39]S. Vijay, T. V. Hogg, J. Ehlers, H. H. Kristoffersen, Y. Katayama, Y. Shao Horn, I. Chorkendorff, K. Chan, and B. Seger, "Interaction of CO with gold in an electrochemical environment," J. Phys. Chem. C **125**(32), 17684–17689 (2021).
[40]H. H. Heenen, J. A. Gauthier, H. H. Kristoffersen, T. Ludwig, and K. Chan, "Solvation at metal/water interfaces: An *ab initio* molecular dynamics benchmark of common computational approaches," J. Chem. Phys. **152**(14), 144703 (2020).
[41]Y. Yoon, R. Rousseau, R. S. Weber, D. Mei, and J. A. Lercher, "First-principles study of phenol hydrogenation on Pt and Ni catalysts in aqueous phase," J. Am. Chem. Soc. **136**(29), 10287–10298 (2014).
[42]M. Zare, M. S. Saleheen, N. Singh, M. J. Uline, M. Faheem, and A. Heyden, "Liquid-phase effects on adsorption processes in heterogeneous catalysis," JACS Au **2**, 2119 (2022).
[43]Z. Yao, G.-J. Xia, W. Cao, K.-H. Zeng, and Y.-G. Wang, "Mechanistic exploration of furfural hydrogenation on copper surface in aqueous phase by DFT and AIMD simulations," J. Catal. **418**, 1–12 (2023).
[44]N. Singh, U. Sanyal, J. L. Fulton, O. Y. Gutiérrez, J. A. Lercher, and C. T. Campbell, "Quantifying adsorption of organic molecules on platinum in aqueous phase by hydrogen site blocking and in situ X-ray absorption spectroscopy," ACS Catal. **9**(8), 6869–6881 (2019).
[45]G. Kresse and J. Furthmüller, "Efficient iterative schemes for *ab initio* total-energy calculations using a plane-wave basis set," Phys. Rev. B **54**(16), 11169–11186 (1996).
[46]B. Hammer, L. B. Hansen, and J. K. Nørskov, "Improved adsorption energetics within density-functional theory using revised Perdew-Burke-Ernzerhof functionals," Phys. Rev. B **59**(11), 7413–7421 (1999).
[47]S. Grimme, J. Antony, S. Ehrlich, and H. Krieg, "A consistent and accurate *ab initio* parametrization of density functional dispersion correction (DFT-D) for the 94 elements H-Pu," J. Chem. Phys. **132**(15), 154104 (2010).
[48]S. Grimme, "Semiempirical GGA-type density functional constructed with a long-range dispersion correction," J. Comput. Chem. **27**(15), 1787–1799 (2006).
[49]S. Sakong, K. Forster-Tonigold, and A. Groß, "The structure of water at a Pt(111) electrode and the potential of zero charge studied from first principles," J. Chem. Phys. **144**(19), 194701 (2016).
[50]H. H. Kristoffersen, T. Vegge, and H. A. Hansen, "OH formation and H_2 adsorption at the liquid water–Pt(111) interface," Chem. Sci. **9**(34), 6912–6921 (2018).
[51]H. H. Kristoffersen, J.-E. Shea, and H. Metiu, "Catechol and HCl adsorption on TiO_2(110) in vacuum and at the water–TiO_2 interface," J. Phys. Chem. Lett. **6**(12), 2277–2281 (2015).
[52]L. Ruiz Pestana, O. Marsalek, T. E. Markland, and T. Head-Gordon, "The quest for accurate liquid water properties from first principles," J. Phys. Chem. Lett. **9**(17), 5009–5016 (2018).
[53]S. K. Natarajan and J. Behler, "Neural network molecular dynamics simulations of solid–liquid interfaces: Water at low-index copper surfaces," Phys. Chem. Chem. Phys. **18**(41), 28704–28725 (2016).
[54]B. Cordero, V. Gómez, A. E. Platero-Prats, M. Revés, J. Echeverría, E. Cremades, F. Barragán, and S. Alvarez, "Covalent radii revisited," Dalton Trans. **21**, 2832–2838 (2008).
[55]P. Gono, F. Ambrosio, and A. Pasquarello, "Effect of the solvent on the oxygen evolution reaction at the TiO_2–water interface," J. Phys. Chem. C **123**(30), 18467–18474 (2019).
[56]A. Serva, M. Salanne, M. Havenith, and S. Pezzotti, "Size dependence of hydrophobic hydration at electrified gold/water interfaces," Proc. Natl. Acad. Sci. U. S. A. **118**(15), e2023867118 (2021).
[57]D. T. Limmer, A. P. Willard, P. Madden, and D. Chandler, "Hydration of metal surfaces can be dynamically heterogeneous and hydrophobic," Proc. Natl. Acad. Sci. U. S. A. **110**(11), 4200–4205 (2013).
[58]R. Šivec, M. Huš, B. Likozar, and M. Grilc, "Furfural hydrogenation over Cu, Ni, Pd, Pt, Re, Rh and Ru catalysts: *Ab initio* modelling of adsorption, desorption and reaction micro-kinetics," Chem. Eng. J. **436**, 135070 (2022).
[59]S. H. Pang and J. W. Medlin, "Adsorption and reaction of furfural and furfuryl alcohol on Pd(111): Unique reaction pathways for multifunctional reagents," ACS Catal. **1**(10), 1272–1283 (2011).
[60]D. Shi and J. M. Vohs, "Deoxygenation of biomass-derived oxygenates: Reaction of furfural on Zn-modified Pt(111)," ACS Catal. **5**(4), 2177–2183 (2015).
[61]Y. Shi, Y. Zhu, Y. Yang, Y.-W. Li, and H. Jiao, "Exploring furfural catalytic conversion on Cu(111) from computation," ACS Catal. **5**(7), 4020–4032 (2015).
[62]S. Wang, V. Vorotnikov, and D. G. Vlachos, "Coverage-induced conformational effects on activity and selectivity: Hydrogenation and decarbonylation of furfural on Pd(111)," ACS Catal. **5**(1), 104–112 (2015).
[63]S. Schnur and A. Groß, "Properties of metal–water interfaces studied from first principles," New J. Phys. **11**(12), 125003 (2009).
[64]J. Le, A. Cuesta, and J. Cheng, "The structure of metal-water interface at the potential of zero charge from density functional theory-based molecular dynamics," J. Electroanal. Chem. **819**, 87–94 (2018).
[65]J.-B. Le, Q.-Y. Fan, J.-Q. Li, and J. Cheng, "Molecular origin of negative component of Helmholtz capacitance at electrified Pt(111)/water interface," Sci. Adv. **6**(41), eabb1219 (2020).
[66]K. Forster-Tonigold and A. Groß, "Dispersion corrected RPBE studies of liquid water," J. Chem. Phys. **141**(6), 064501 (2014).
[67]D. S. Potts, D. T. Bregante, J. S. Adams, C. Torres, and D. W. Flaherty, "Influence of solvent structure and hydrogen bonding on catalysis at solid–liquid interfaces," Chem. Soc. Rev. **50**, 12308 (2021).
[68]A. J. Medford, J. Wellendorff, A. Vojvodic, F. Studt, F. Abild-Pedersen, K. W. Jacobsen, T. Bligaard, and J. K. Nørskov, "Assessing the reliability of calculated catalytic ammonia synthesis rates," Science **345**(6193), 197–200 (2014).
[69]S. R. Kelly, H. H. Heenen, N. Govindarajan, K. Chan, and J. K. Nørskov, "OH binding energy as a universal descriptor of the potential of zero charge on transition metal surfaces," J. Phys. Chem. C **126**, 5521 (2022).
[70]X.-Y. Li, A. Chen, X.-H. Yang, J.-X. Zhu, J.-B. Le, and J. Cheng, "Linear correlation between water adsorption energies and Volta potential differences for metal/water interfaces," J. Phys. Chem. Lett. **12**(30), 7299–7304 (2021).
[71]A. E. G. Mikkelsen, J. Schiøtz, T. Vegge, and K. W. Jacobsen, "Is the water/Pt(111) interface ordered at room temperature?," J. Chem. Phys. **155**(22), 224701 (2021).
[72]C. Schran, F. L. Thiemann, P. Rowe, E. A. Müller, O. Marsalek, and A. Michaelides, "Machine learning potentials for complex aqueous systems made simple," Proc. Natl. Acad. Sci. U. S. A. **118**(38), e2110077118 (2021).
[73]J. Vandermause, Y. Xie, J. S. Lim, C. J. Owen, and B. Kozinsky, "Active learning of reactive Bayesian force fields applied to heterogeneous catalysis dynamics of H/Pt," Nat. Commun. **13**(1), 5183 (2022).
[74]M. F. Calegari Andrade, H.-Y. Ko, L. Zhang, R. Car, and A. Selloni, "Free energy of proton transfer at the water–TiO_2 interface from *ab initio* deep potential molecular dynamics," Chem. Sci. **11**(9), 2335–2341 (2020).
[75]Z. An and J. Li, "Recent advances in catalytic transfer hydrogenation of furfural to furfuryl alcohol over heterogeneous catalysts," Green Chem. **24**, 1780 (2022).
[76]Y. Kwon, K. J. P. Schouten, J. C. van der Waal, E. de Jong, and M. T. M. Koper, "Electrocatalytic conversion of furanic compounds," ACS Catal. **6**(10), 6704–6717 (2016).